Available online at www.sciencedirect.com
SCIENCE DIRECT®
Acta Materialia 52 (2004) 4317–4328
Acta MATERIALIA
www.actamat-journals.com

Dislocation study of prismatic slip systems and their interactions in hexagonal close packed metals: application to zirconium

G. Monnet *, B. Devincre, L.P. Kubin

Laboratoire d'Etude des Microstructures, CNRS-ONERA, 29 av. de la Division leclerc, BP72, 92322 Châtillon Cedex, France

Received 4 July 2003; received in revised form 27 May 2004; accepted 28 May 2004
Available online 19 June 2004

Abstract

Simulations of dislocation dynamics in single crystals of hcp zirconium are presented with emphasis on the hardening associated with prismatic slip at low temperature. Two original aspects of the simulation method are discussed, the treatment of the hcp lattice by an orthorhombic representation and the use of periodic boundary conditions. The mobility of screw and non-screw segments are defined in a phenomenological manner. Different investigations on the interactions between dislocations gliding in different prismatic planes show that no junction is formed between intersecting screw dislocations, which results in a rather small forest hardening at low temperature. This explains experimental observations of an initial deformation stage with a low strain hardening coefficient in zirconium or titanium crystals at low temperature.

Keywords: Dislocation dynamics; Strain hardening; Prismatic slip; Simulation; Zirconium

1. Introduction

The present paper is devoted to a simulation study of forest and strain hardening in zirconium crystals deforming by prismatic slip. The plastic deformation of Zr single crystals has been the object of many early studies. Whatever the temperature, prismatic slip is the dominant deformation mode [1]. Secondary deformation modes are mechanical twinning at low temperature [2], and basal and $\langle c+a \rangle$ slip at high temperature [3]. In addition, pyramidal slip is sometimes observed and its activity increases with increasing temperature [6]. The conditions for the operation of these hard slip modes are poorly known, especially at low temperatures, as illustrated by continuum models for polycrystal plasticity and texture simulations (see e.g. [4,5]). In the present study, we exclusively consider dislocation glide in the prismatic planes.

In zirconium, as well as in titanium, which behaves in quite a similar manner, the flow stress is strongly temperature dependent [7–9] and the microstructures of deformed specimens mainly contain long and straight screw segments [6] (see also [10] and references therein for *in situ* studies of prismatic slip in several hcp metals by transmission electron microscopy). Atomistic simulations showing a three-dimensional spread of the screw dislocation cores [11,12], also confirm the presence of a significant lattice friction on screw dislocations. At the mesoscale, the mobility of screw dislocations and its temperature and strain rate dependencies can be modeled in terms of the kink-pair mechanism [13], embedded into the framework of thermally activated deformation [14]. Another contribution to dislocation mobilities stems from a rather strong sensitivity to trace amounts of interstitial impurities, the origin of which has not yet been clarified [7–9,15].

These aspects cannot be investigated at the mesoscopic scale and will be considered in what follows as input properties. On the other hand, strain hardening properties are related to dislocation interactions, which can be treated within an elastic framework and are, therefore, suited for mesoscale analyses.

In the absence of experimental data on pure material, dislocation dynamics (DD) simulations specifically

* Corresponding author. Present address: EDF – MMC, Avenue des Renardières, 77818 Moretsur Loing, France. Tel.: +33-1-46-73-44-49; fax: +33-1-46-73-41-55/60-73-68-89.

1359-6454/$30.00 © 2004 Acta Materialia Inc. Published by Elsevier Ltd. All rights reserved.
doi:10.1016/j.actamat.2004.05.048

designed for Zr single crystals can be used to check several aspects of the mechanical response. A first step in this direction is presented here. The first three-dimensional DD simulation specifically devoted to crystals with hexagonal symmetry and its application to Zr single crystals is presented in Section 2. As discussed in Section 3, the mobility laws for screw and non-screw segments are implemented by combining current phenomenology and the available experimental data. The interactions between prismatic slip planes and the resulting forest and strain hardening properties are then investigated in Section 4 and discussed in Section 5.

2. Dislocation dynamics simulations

The DD simulation used in the present study is described in several publications [16,17]. For this reason, only features that are specific to the present work are recalled in this section. Two important aspects are detailed, namely the treatment of the hexagonal symmetry and the monitoring of the mean free-path of dislocations using periodic boundary conditions (PBCs).

2.1. The discrete model

Line discretization and the definition of a three-dimensional lattice tiling an elastic continuum constitute the two essential features of the present DD simulation. Like in other existing simulations [18–20], dislocation lines are decomposed in a piecewise manner but, in the present case, the segments considered are constrained to lie on a lattice that discretizes the simulated volumes. Then, by construction, the dislocation segments can only take a finite number of characters. In practice, only the $[0\,0\,0\,1]$ edge, $\langle 2\,-1\,-1\,0\rangle$ screw and two mixed line directions are taken into account in each slip system. The two mixed directions are needed in order to further treat reactions between prismatic slip and another slip system [21], for instance the pyramidal one. Line discretization decreases the number of degrees of freedom to be accounted for during the displacement of the dislocation lines; it results in a better computing efficiency without loss of accuracy [17,21].

The incremental time steps of the simulation are divided into two parts. Firstly, dislocations are treated as purely elastic defects. The effective force on each segment is computed at its midpoint as a superposition of several contributions. The latter include the Peach–Koehler forces derived from the applied stress, the stress fields of other dislocation segments [22] and a local line tension term taken from the classical work by Foreman [23]. To estimate the resulting displacement of the segments, a mobility law is required. The definition of mobility laws is an important input of DD simulations, especially in the presence of lattice friction. This particular aspect deserves a specific discussion, which is given in Section 3.

Secondly, the positions of the dislocation segments are updated using a procedure that accounts for possible local events occurring during their displacement. These events include direct annihilation with other dislocations, junction formation with non-coplanar dislocations [24] and cross-slip, for which specific local rules are implemented [16]. Therefore, although this is not relevant to the present study, the DD simulation can treat cross-slip from prismatic planes to a secondary slip system and the mutual interaction of these two slip systems.

Finally, well-known limitation of DD simulation originates in the small value of the maximum plastic strain that can be reached, typically a few 10^{-3}. This is due to the fast increase of the number of interacting dislocation segments during plastic straining.

2.2. Hexagonal symmetry

The crystallography of the hcp lattice traditionally makes use of the four Miller–Bravais indices, *hkil*, attached to the four-axis system $\{\overrightarrow{a_1}, \overrightarrow{a_2}, \overrightarrow{a_3}, \overrightarrow{c}\}$, where $\overrightarrow{c}$ is the axis of six-fold symmetry and the three others axes are lying in the basal plane. This representation is unfortunately not appropriate for DD simulations. It implies handling one additional index with respect to cubic notations and abandoning all the advantages of orthogonality for arithmetic computations. Alternatively, one can use a set of cubic axes and three real indexes, but these coordinate axes do not coincide with those used to discretize the dislocation segments, which makes them fully inconvenient. An alternative solution, which is compatible with our lattice-based approach, has been adopted. It makes use of the orthorhombic description of the hexagonal cell [25,26], which is widely used for numerical calculations in hexagonal lattices. The basal plane is indexed as a $(1\,1\,1)$ plane and the $\overrightarrow{a}$ directions become $\langle 1\,1\,0\rangle$ directions, like in the fcc structure. The transformation matrix from the 4D-space generated by the classical Miller–Bravais indices to this new 3D coordinate system is written:

$$M = 22\begin{pmatrix} 0 & 3 & \overline{3} & 4 \\ 3 & \overline{3} & 0 & 4 \\ \overline{3} & 0 & 3 & 4 \end{pmatrix}. \tag{1}$$

The scaling factor of 22 is introduced here to ensure that all the elementary vectors of the simulation have integer value in the orthorhombic set of axes. For example, the matrix M allows transforming the Burgers vectors $\overrightarrow{a_1} = 1/3[2\,\bar{1}\,\bar{1}\,0]$ and $\overrightarrow{a_2} = 1/3[\bar{1}\,2\,\bar{1}\,0]$ and the direction $\overrightarrow{c} = [0\,0\,0\,1]$, into the new vectors: $\overrightarrow{t_1} = 66[0\,1\,\bar{1}]$, $\overrightarrow{t_2} = 66[1\,\bar{1}\,0]$, and $\overrightarrow{t_3} = 88[1\,1\,1]$. In this new set of coordinates, the discretization length of the screw segments, i.e., their minimum length, L_s, is set to

$L_s = |\langle 1\,1\,0\rangle| = 2$ nm. For edge segments, the corresponding value is $L_e = 3.26$ nm. These small segment's lengths allow treating in an accurate manner the curvature radii of non-screw segments under stress. The above transformation of axes assumes an ideal hexagonal cell ($c/a = \sqrt{8/3}$). In the case of Zr or Ti, where this ratio is about 1.59, the transformation involves a small distortion of the elastic continuum of about 2.7% along the $\vec{c}$ axis. The resulting error, for instance in the Peach–Koehler force, is at most of same order and can be neglected.

2.3. Periodic boundary conditions

The implementation of PBCs in DD simulation was proposed and discussed by Bulatov et al. [27]. These conditions make use of a simulation cell and a set of replicas. Every time a dislocation segment crosses a boundary between two cells, a replica of it emerges in all cells at the equivalent position in the opposite boundary (cf. Fig. 1). There is, however, a known problem associated with PBCs, specifically that of the self-reactions of portions of dislocation loops with their replicas after a certain glide path over the extended simulation volume. This distance is a complex function of the dimensions of the simulation cell, of the slip geometry and of the shape, isotropic or anisotropic, of the expanding dislocation loops. A general solution has been developed to control this artifact and prescribe a minimum value for the self-reaction distance of the order of the relevant mean-free path. It is based on an adequate choice of the dimensions of the primary cell, which is no longer cubic but orthorhombic [28]. Only the particular case of Zr at low temperature, i.e., of strongly anisotropic dislocation loops, is examined here.

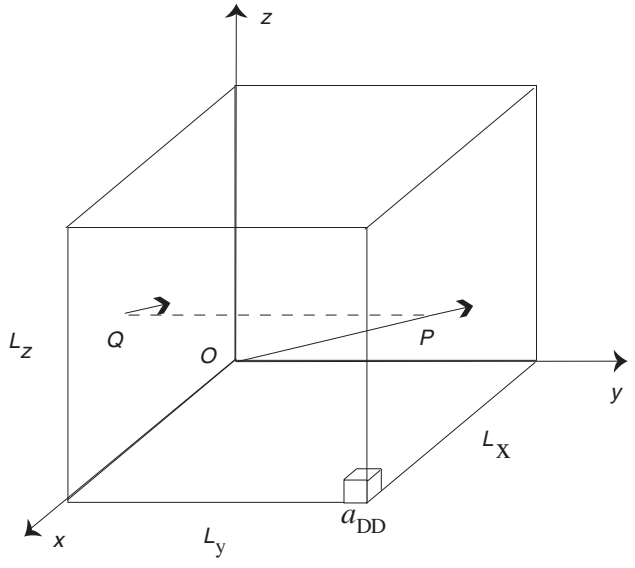

Fig. 1. When a small edge segment propagating along OP crosses the boundary of a simulation cell to enter another cell, a replica of it is reintroduced at a position defined by a translation, here $PQ = -L_y$, in order to balance the dislocation flux. The dimensions of the cell are L_x, L_y, L_z and a_{DD} is the parameter of the underlying lattice, which governs the length scale of the simulation.

At low temperature in Zr, screw dislocations have a low mobility in the prismatic planes, as compared to the non-screw segments that experience a comparatively much smaller lattice friction. Hence, the non-screw segments can travel long distances and the dislocation loops are elongated along the direction of their Burgers vector. The self-interaction distance, λ, to be controlled is then that of non-screw segments propagating along the screw direction in the prismatic planes.

The dimensions of the orthorhombic simulation cell, (L_x, L_y, L_z), are integer multiples of the dimensions of the simulation lattice $a_{DD} : L_x = N_x a_{DD}, L_y = N_y a_{DD}$ and $L_z = N_z a_{DD}$ (cf. Fig. 1). The unit glide direction of the short edge segments is $\vec{d} = (d_x, d_y, d_z)$ and the corresponding glide path is represented by a vector $\overrightarrow{OP}$, starting from the origin O and of increasing magnitude $l : \overrightarrow{OP} = l\,\vec{d}$. With increasing time, the small portion of dislocation line represented by P repeatedly crosses the periodic boundaries. Every time this happens, a new replica of P starts gliding into a new slip plane, as a result of translations along the three Cartesian axes, like the one shown in Fig. 1. Eventually, after a number (u, v, w) of boundary crossings and translations along the three Cartesian directions, P returns to its original position or a replica of it. Thus, the condition for self-reaction, is written:

$$\begin{cases} ld_x - uN_x = 0, \\ ld_y - vN_y = 0, \\ ld_z - wN_z = 0. \end{cases} \tag{2}$$

By eliminating l, one obtains two independent relations:

$$\begin{cases} u = \frac{N_y d_x}{N_x d_y} v, \\ v = \frac{N_z d_y}{N_y d_z} w. \end{cases} \tag{3}$$

This set of equations has an infinite number of solutions for integer values of (u, v, w). The first self-reaction event is the physically meaningful one; it corresponds to the smallest non-zero integer solution (u_0, v_0, w_0) of the set of Eqs. (3). One then has:

$$\lambda = \sqrt{(u_0 L_x)^2 + (v_0 L_y)^2 + (w_0 L_z)^2}. \tag{4}$$

For an elongated loop expanding in two opposite directions, Eq. (4) represents the total self-annihilation diameter, i.e., twice the self-interaction path of each extremity. From this simple result, we see that the lengths $u_0 L_x$, $v_0 L_y$ and $w_0 L_z$ define the dimensions of a

virtual extended crystal such that a dislocation loop expanding from its center gets annihilated when reaching its boundaries. As a result, the dimensions of this virtual crystal can be adjusted by selecting adequate cell dimensions for a given slip system in order to impose any prescribed self-annihilation distance.

Due to the high Peierls stress, it is not possible to simultaneously activate the three prismatic slip systems in single crystals. Then, it is sufficient to control only two mean-free paths. For instance, with an orthorhombic simulation cell of reduced dimensions $N_x = N_y = 3/2N_z = 3564$, and with $a_{DD} = 0.343 \times 10^{-8}$ m, the solutions of Eq. (4) are ($u = 0,\ v = -2,\ w = 3$) and ($u = -2,\ v = 0,\ w = 3$), for short non-screw segments propagating along the screw direction in the two prismatic planes $P_I = (0\bar{1}10)[2\bar{1}\bar{1}0]$ and $P_{III} = (\bar{1}100)$ $[\bar{1}\bar{1}20]$, respectively. The mean free-path has then the same value in the two systems, $\lambda = 2\sqrt{2}N_x a_{DD} \approx 34$ μm. These values are the ones adopted in this work for the study of duplex slip in prismatic planes (cf. Section 3.2).

3. Mobility laws

3.1. Screw dislocations

A typical Arrhenius form suited for representing dislocation motion by a kink-pair mechanism is written [14]:

$$v(\tau^*, T) = v_0 \frac{l}{l_0} \exp\left(-\frac{\Delta G(\tau^*)}{kT}\right), \tag{5}$$

where, v is the velocity of a straight screw dislocation segment of length l between strong obstacles to kink motion, $\Delta G(\tau^*)$ is the activation free-energy under the effective shear stress τ^* at the absolute temperature T and k is the Boltzmann's constant. The velocity v_0 is a constant, which includes a Debye frequency and other terms [30], and l_0 is a scaling length. The proportionality of the velocity to the segment's length accounts for the number of potential nucleation sites in competition for each kink-pair nucleation event. The prefactor is not strictly speaking a constant, but its variations are negligible as compared to those of the exponential term.

Following a method previously developed for the simulation of Dislocation dynamics in bcc metals [29,30], use was made of a phenomenological form for the activation free energy associated with dislocation–obstacle interactions [31]:

$$\Delta G(\tau^*) = \Delta G_0 \left(1 - \left(\frac{\tau^*}{\tau_0}\right)^p\right)^q, \tag{6}$$

ΔG_0 is the total activation free energy, τ_0 the Peierls stress at 0 K and p and q are free parameters. The unknown parameters in Eqs. (5) and (6) were fitted to experimental data on single crystals obtained by Mills and Craig [8]. We obtained: $v_0 = 1600$ m/s, $l_0 = 5$ μm, $p = 0.757$ and $q = 1.075$. $\tau_0 = 262$ MPa $= 5.8 \times 10^{-3}\mu$ (where $\mu = 45$ GPa is the shear modulus of zirconium extrapolated at the absolute zero of temperature). The total activation energy is $\Delta G_0 = 1.06$ eV, or $0.12\mu b^3$ (with a basal Burgers vector $b = 0.323$ nm). These values are in agreement with experimental determinations [7,8] and the reduced values are of same order of magnitude as those found in bcc metals [29,30].

In the present work, we assumed that the effect of interstitial impurities present in the material tested by Mills and Craig [8], which is about 1200 wt. ppm, is incorporated into the above stress vs. velocity law for screw dislocations. In Ti or Zr, it was shown by Tyson [33] (see also [9]) that there is no net elastic interaction energy between a perfect screw dislocation and a solute atom inducing a tetragonal distortion. It has been suggested that the interaction between screw dislocations and interstitial solutes is chemical in nature and induces a modification of the core structure of screw dislocations and of the resulting energetic of kink-pair nucleation rate, whereas propagating kinks probably also interact with solute atoms. These hypotheses, which have not yet been confirmed by atomistic simulations, are implicit in the present treatment of the screw dislocation velocities.

3.2. Non-screw segments

The non-screw segments have a much larger mobility than the screw ones, as experimentally attested by the highly anisotropic shapes of expanding dislocation loops (cf. Section 4.2 and Fig. 3(c)). This indicates that their interaction with interstitial solutes has a weaker effect on their mobility than the Peierls force has on the mobility of screw dislocations. Their dynamics involves two unknown quantities: their mean free-flight distance, λ, and their velocity, which depends in principle on stress and temperature. A range of plausible values for these two parameters was obtained by considering their coupled influence on the simulated microstructures and the stress–strain curves.

Non-screw dislocations are responsible for the occurrence of a small pre-yield deformation at stress levels below the critical resolved shear stress (CRSS), i.e., before the onset of screw dislocation motion (cf. Fig. 2). In the DD simulation and below the macroscopic yield stress, the non-screw segments are mobile and are seen to trail long dipoles of sessile screw segments. This effect is well documented in pure bcc crystals [30], much less in Ti or Zr crystals, due to usually high impurity contents. No estimate is available for the related mean-free path but it seems reasonable to assume that it is governed by strong obstacles like sub-grain boundaries, other dislocations, or simply the free surfaces of the specimen. Assuming too great value for the mean free-path λ would result in an unrealistically large amount of pre-

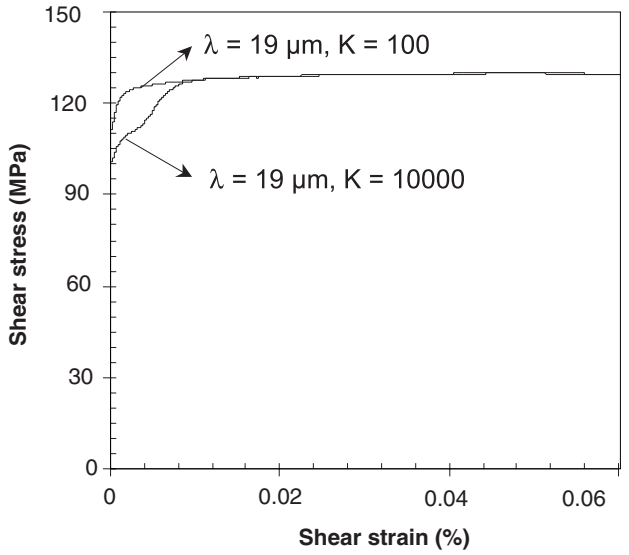

Fig. 2. Influence of K, the ratio of non-screw to screw velocities, on the simulated stress–strain response. The temperature is 300 K and the constant imposed strain rate is 10^{-3} s^{-1}. λ is the mean free-path of the non-screw dislocations.

yield deformation given by non-screw segments. With too short a value, long screw segments would no longer be obtained. In the absence of any numerical data, it was assumed that λ is at least one order of magnitude larger than the average distance between dislocations. As this last distance is in the μm range, an appropriate value of λ is typically a few tens of micrometers. This value was implemented into the DD simulation via the PBCs (cf. Section 2.3).

Several types of stress vs. velocity laws were tested for the mobility of the non-screw segments. They were found not to affect the flow stress as long as the mobility of non-screw segments was substantially larger than that of screw segments. For the sake of simplicity, the mobilities of the two types of segments were assumed to be proportional to each other, with a proportionality constant K.

Fig. 2 shows simulated stress–strain curves at 300 K for two different values of K, $K = 100$ and $K = 10,000$ and with a mean free-path of 19 μm for the non-screw segments. One can see that a substantial change in the value of K does not alter the yield stress, which confirms that the latter is governed by the onset of screw dislocation motion. However, such a change affects the pre-yield stage: as expected, the pre-yield deformation increases with increasing non-screw mobility. With very high values of K, however, the time step of the simulation has to be reduced, due to the increase in the velocity of non-screw segments, which results in a loss of computing efficiency. With values of K smaller than 100, dislocation loops tend to become less anisotropic than experimentally observed [6]. All these dependencies are not significantly affected if the value of λ is modified within the previously defined range. As a result of this preliminary study, all the simulations of plastic deformation were carried out with $K = 1000$ and $\lambda = 34$ μm.

4. Simulation results

4.1. Initial configurations

The initial configurations used in DD simulation attempt to mimic those of annealed specimens. The orthorhombic reference cell has linear dimensions of about 10 μm. It initially contains a random distribution of Frank–Read sources on the three prismatic slip systems. All the sources are of edge character and their total density is about 10^{-3} m^{-2}. The simulations reported here were carried out with a tensile axis parallel to $\overrightarrow{a_2}$, which activates duplex slip on the two prismatic systems P_{I} and P_{III} with a Schmid factor of 0.433. These symmetrical conditions are the simplest ones that allow characterizing the forest interactions between two prismatic slip systems.

4.2. Simulated microstructures

An example of a simulated microstructure at $T =$ 300 K is shown in Fig. 3(a). After a plastic strain $\epsilon_{\mathrm{p}} =$ 0.2%, obtained by imposing a constant total strain rate of $\dot{\gamma} = 10^{-4}$ s^{-1}, a uniform dislocation density of 1.5×10^{12} m^{-2} is obtained. As expected from the loading conditions, this microstructure is mostly composed of dislocations belonging to the systems P_{I} and P_{III}.

More detail can be seen in a thin foil extracted from the simulation and parallel to the basal plane (cf. Fig. 3(b)). The prismatic planes are normal to the foil and their projections are parallel to the Burgers vectors. The microstructure consists of a random array of long screw dislocation segments on the two active slip systems. Close inspection of the simulated microstructures reveals that very few junctions are formed between the two active slip systems, and none between screw dislocations. Similar dislocation configurations were found all through the low temperature range. They are a direct consequence of the low mobility of the screw dislocations. For comparison, Fig. 3(c) reproduces a transmission electron micrograph from a Zr polycrystal plastically deformed at 300 K (after [6]). (Fig. 3(d)) shows a high-temperature microstructure obtained by attributing to both screw and non-screw segments a Newtonian stress vs. velocity relationship typical of metals where the dislocation velocity is governed by phonon damping [16,17]. In such conditions, the microstructure presents many similarities with those observed in fcc crystals: the screw dislocations are no longer straight; they bow-out under stress and the dislocation loops exhibit isotropic shapes. In addition,

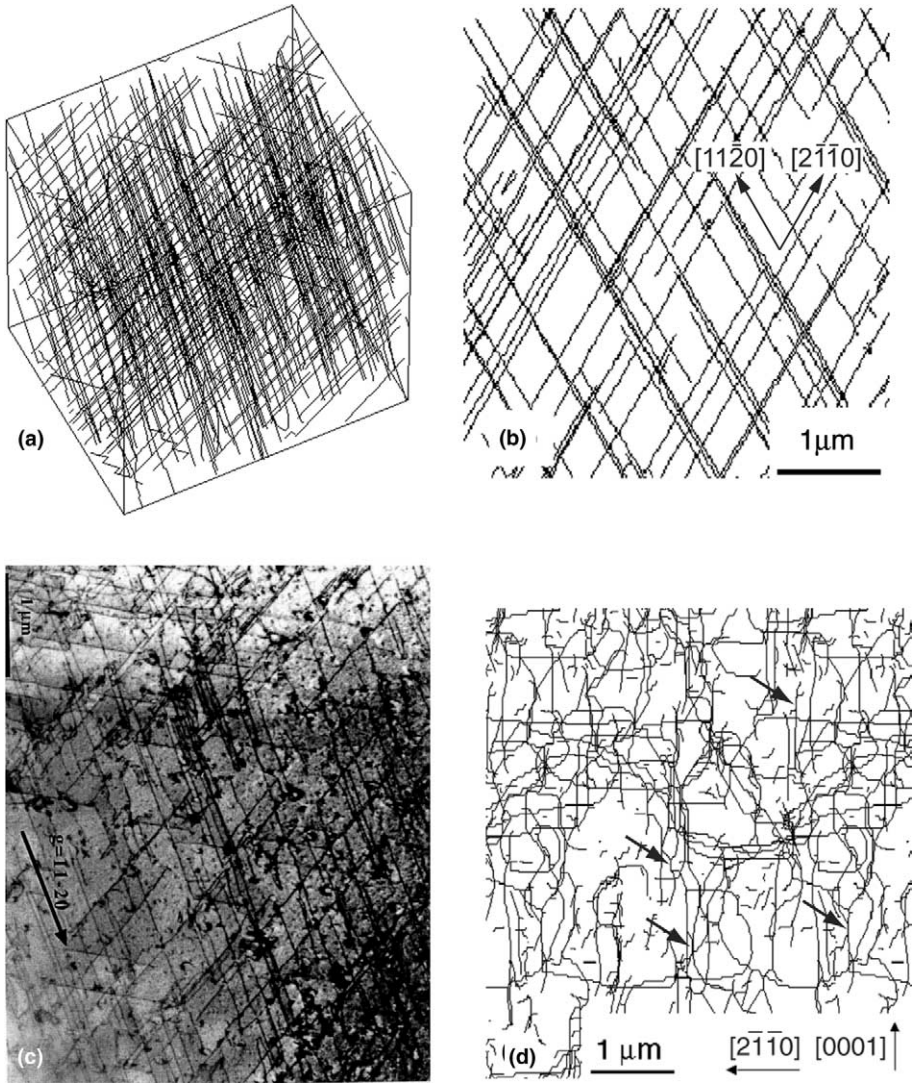

Fig. 3. (a) Simulated dislocation microstructure after a tensile test in duplex slip conditions with a constant imposed strain rate of 10^{-4} s^{-1} ($T = 300$ K, $\epsilon_p = 0.2\%$). (b) A thin foil of thickness 1 μm cut from the simulation cell (a) along the basal plane. The microstructure essentially consists of elongated screw segments developed on the two activated prismatic slip systems. (c) Transmission electron micrograph showing a similar microstructure in a zirconium polycrystal after 2% plastic strain at 300 K with a constant applied strain rate of 5×10^{-5} s^{-1} [6]. (d) A simulated high-temperature microstructure with isotropic velocities for screw and non-screw dislocations. The thin foil, of thickness 1 μm, is parallel to one of the active prismatic slip planes. The arrows point at junction configurations.

junction formation is observed to occur, principally between non-screw segments.

4.3. Thermally activated properties

The evolution of the CRSS with temperature under a constant applied strain rate of 10^{-3} s^{-1} is shown in Fig. 4 and compared with the experimental data that served to calibrate the mobility rule for screw dislocations (cf. Section 3.1). An athermal alloy friction of 20 MPa was added to the glide resistance in order to match the experimental value of the CRSS at high temperature. The excellent coincidence confirms, indeed, that the Arrhenius form describing the mobility law of the screw dislocations fully reproduces the low temperature dependence of the macroscopic CRSS in Zr.

For temperature above 470 K, however, the simulation results start departing from the experimental data (this can be seen from the data points at 520 K in Fig. 4). Close to the so-called athermal temperature of 580 K, where the lattice friction is no longer significant, the mobility of screw dislocations becomes comparable to that of non-screw dislocations [8]. To account for this transition domain, the constant velocity ratio K should be made temperature-dependent. For instance, taking smaller K-values (typically less than 10) in this temperature range, one obtains as expected, rather different dislocation microstructures, similar to the one shown in

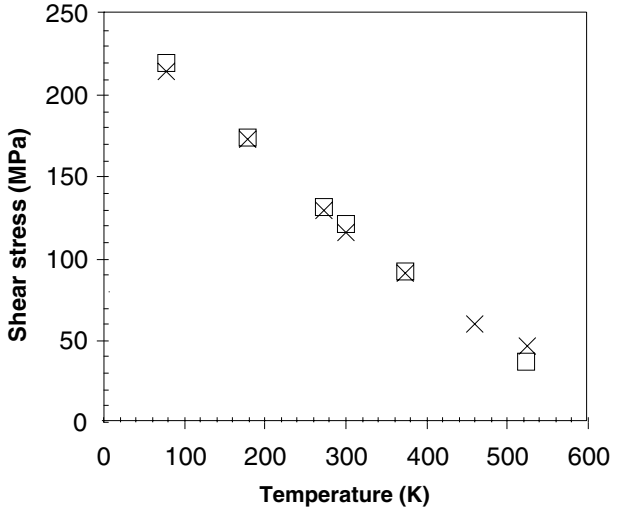

Fig. 4. Temperature dependence of the CRSS under a constant imposed strain rate of 10^{-3} s^{-1}. The simulation results ($\times$) are compared to the experimental values [8] used to calibrate the velocity of screw dislocation segments ($\square$).

Fig. 3(d). Hence, a transition is obtained from the low temperature regime to a high temperature regime governed by dislocation intersections and characterized by primarily athermal processes.

The influence of strain rate on the mechanical response was also tested. Simulation results obtained at $T = 300$ K and with three different imposed strain rates are shown in Fig. 5. The strain rate sensitivity of the yield stress is, as expected, fully consistent with the sensitivity of the screw dislocation velocities to the effective stress, as deduced from the imposed velocity rule (cf. Section 3.1). For instance, the value of the activation volume, V, can be deduced from Fig. 5, by measuring the stress difference associated with a change in strain rate by a factor of 10, in conditions of constant dislocation density (i.e., at the stress maxima). One finds $V \approx 22b^3$, whereas the input value deduced from Eq. (6) is $V = -\mathrm{d}\Delta G(\tau^*)/\mathrm{d}\tau^* = 19b^3$.

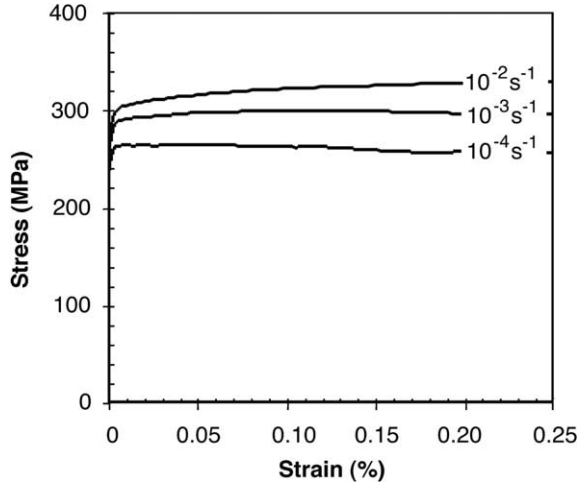

Fig. 5. Simulated stress–strain curves obtained at $T = 300$ K and with three different imposed strain rates. The simulation conditions are the same as in Fig. 4.

The two checks presented above, and others that are not reported here, simply show that, just like in the case of bcc metals [32], the thermally activated properties of the simulated mechanical response are the same as those implemented in the velocity law for screw dislocations (Eqs. (5) and (6)). In the absence of any theoretical prediction of the screw dislocation mobilities, a fitting procedure such as the one utilized here is unavoidable. It allows, nevertheless, performing a study of the mesoscopic response related to the forest and strain hardening properties.

4.4. Forest hardening

Beyond the yield stress, the dislocation density increases continuously and dislocation intersections and reactions become more frequent. Quite generally, the corresponding increase in glide resistance is thought to be responsible for strain hardening. However, no measurable work hardening was yielded by the present DD simulations in the low temperature range, as can be checked from Fig. 5. In contrast, a smooth yield point was systematically recorded, inducing some softening either just after the yield stress or after a variable amount of strain. This feature is associated with a continuous multiplication of the screw dislocations and an absence of storage, leading to a plastic strain rate that slightly increases above the nominal value. This seems to indicate that the interaction between prismatic slip systems does not harden the crystal. To understand this unexpected result, the strength of the prismatic forest was examined by two different methods. An interaction mapping was constructed, which describes the domain of junction formation for different possible geometrical configurations. It is emphasized that, owing to the purely elastic nature of the processes investigated, these simulations are parameter-free. Further, model simulations of latent hardening were performed to quantify the contribution of the forest density to the flow stress.

4.4.1. Interaction mapping

The orientation dependence of the interaction between two initially straight, non-coplanar, segments gliding in two different prismatic planes has been simulated. For more detail on the procedure used, the reader is refereed to a recent systematic study performed on bcc and fcc metals [34]. Fig. 6(a) shows the mapping obtained for the interaction of two segments of initial length 10 μm and with variable orientations, in a graphical representation similar to the one used by Wickham et al. [35] for bcc metals and Madec et al. [36] for fcc metals. The orientation of the lines are defined by their angles φ_1 and φ_2 with respect to [0001], the

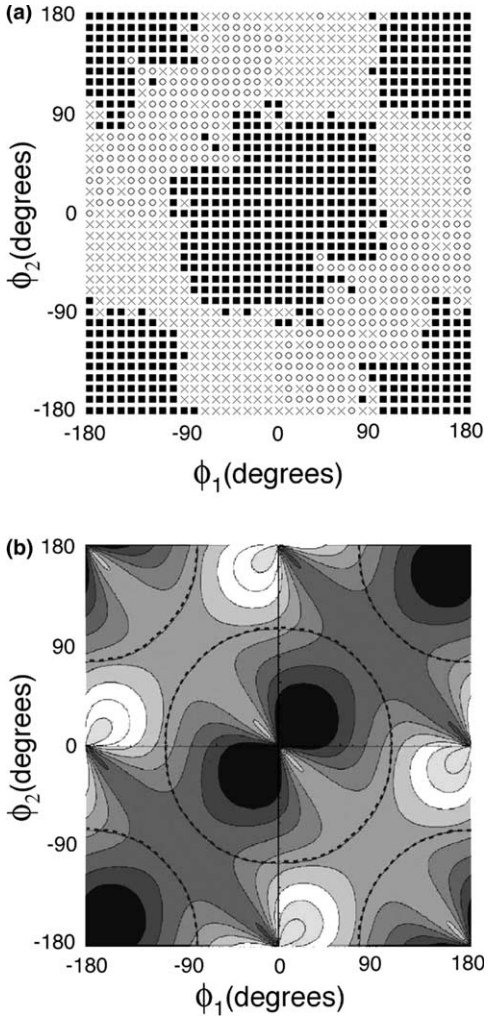

Fig. 6. Interaction mapping for two dislocation segments of length 10 μm in two intersecting prismatic planes. The angles φ_1 and φ_2 define the orientation of the lines with respect to the intersection of the two slip planes. (a) Simulation results (filled rectangles, crosses and open circles refer to junction formation, crossed-state and repulsive crossing, respectively). (b) Elastic prediction for the interaction force of two infinite and straight dislocations (see text for detail).

direction at the intersection of the two slip planes. After relaxation of the initial configuration, three types of configurations are obtained: (i) when the elastic interactions are strong and attractive, junction formation occurs. (ii) Repulsive configurations are observed in some other regions of the mapping, and (iii) when the interaction is weak, either local pinning occurs or the nature of the interaction, attractive or repulsive, cannot be defined. These last states are called cross-states [35,36]. Each final configuration is in equilibrium under zero applied stress and does not depend on kinetics. In other terms, the equilibrium states are independent of the lattice friction and correspond to the configuration formed in a real crystal at high temperature.

In Fig. 6(b), two predictions obtained using simplified elastic models [36,34], are shown. They aim at providing a check from elastic solutions less sophisticated than those yielded by the simulation. The dashed, approximately circular domains enclose areas where junction formation induces a reduction of the elastic line energy of the whole configuration. This condition is calculated for straight segments, in isotropic elasticity and with an orientation-dependent line tension that does not include a logarithmic term (this last term is, indeed, accounted for in the simulations). The set of contour levels in gray shades represent iso-interaction forces (white corresponds to strong repulsion and black to strong attraction) along the shortest approach distance of two rigid, infinite dislocations. This last calculation was performed using a simple solution given by Kroupa [37].

The comparison between Fig. 6(a) and (b) shows that, like in other crystal structures, junction formation can be qualitatively predicted by an energetic criterion. This criterion is, however, slightly in defect when the two segments are initially repulsive, which clearly shows the limits of too simple elastic models [34]. Junctions between prismatic systems are always formed when the dislocation lines are the most attractive and make a small angle with respect to the intersection of the slip planes and with each other. This maximizes their interaction, which results in junction formation inside a closed domain centered on the origin and its periodic duplicates. The edge direction $[0\,0\,0\,1]$ is located at the center of these domains, where the junction strength is maximum. On the other hand, one can note that the regions corresponding to the intersection of two screw lines, $\varphi_1 = \pm 90°$ and $\varphi_2 = \pm 90°$, are always outside the domain of junction formation.

During the plastic deformation of Zr crystals at low temperature, the dominant component of the dislocation density is of screw character. It is, therefore, not likely to form junctions through forest interactions, irrespective of the kinetics of the process. The short and highly mobile non-screw segments have a quite small probability of mutual interaction, whereas the intersections of screw and non-screw segments are found at the periphery of the domain of junction formation, which means that they constitute a weak obstacle. Hence, very little forest hardening is expected to occur at low temperature, in agreement with the results reported in Fig. 5 and the absence of junctions in the simulated microstructures (Fig. 3(b)).

At high temperature, in contrast, the hardening due to the prismatic forest should not be much different from the typical stage II behavior of fcc crystals, since the mapping shown in Fig. 6(a) is not much different from the one found for e.g., Lomer locks [36].

4.4.2. Model simulations of forest hardening

In order to substantiate the information provided by the interaction mapping, model simulations of forest hardening were performed. The aim of those

computations is to investigate, in dynamic conditions involving an applied stress and the effect of the lattice friction, the contribution from several types of intersections to the glide resistance. Fig. 7(a) and (b) shows the configurations adopted by long dislocation lines of initially edge or screw character upon moving across a density of intersecting dislocations. These simulations were carried out by imposing a constant strain rate of 10^{-5} s^{-1}. The forest density was set to 10^{12} m^{-2} and it only contained screw dislocations, since the majority of dislocations in the microstructure have that character. The applied resolved stress on the forest slip system was set to zero in order to prevent the forest density from multiplying under stress.

A mobile line of initially edge character acquires a distinct roughness during its motion, which shows that it is, indeed, strongly pinned by junctions formed with forest obstacles. These junctions induce local bowed-out configurations that tend to align themselves along the screw direction (cf. Fig. 7(a)). According to the results of Fig. 6, the interaction between screw and edge dislocation is located at the periphery of the junction lobe and results in a weak junction. However, when the lines that bow out during the unzipping process reach the screw orientation, they form small segments of screw orientation (cf. arrows in Fig. 7(a)). Since these screw segments have a low mobility, they delay the destruction of the junction and increase the effective junction strength with respect to its value at high temperature.

The length of the junctions, reduced by the average distance between forest obstacles, is shorter than predicted by simplified energetic arguments. This is due to the effect of the applied stress, which reduces the equilibrium length of junctions and also to a kinetic effect. The forest dislocations of screw character have a low mobility and the junctions are unzipped under stress before having reached their maximum extension.

Gliding screw dislocations do not exhibit any marked roughness (Fig. 7(b)) and do not form stable junctions with the forest dislocations, as expected. Only a few superkinks are observed to form on the screw lines as a result of the strong local elastic interactions occurring when lines are crossing each other. Hence, the propagation of screw dislocation lines in prismatic slip planes is mostly insensitive to prismatic forest obstacles, except in the occasional cases where the latter are of non-screw character.

Fig. 8 synthesizes these results by showing the stress–strain responses associated with the model simulations shown in Fig. 7(a) and (b) (curves 1 and 3), to which are added two curves obtained in the absence of forest dislocations, for mobiles lines of screw and edge character (curves 2 and 4, respectively). After a transient stage, the stress saturates at a level that is sensitive to the presence

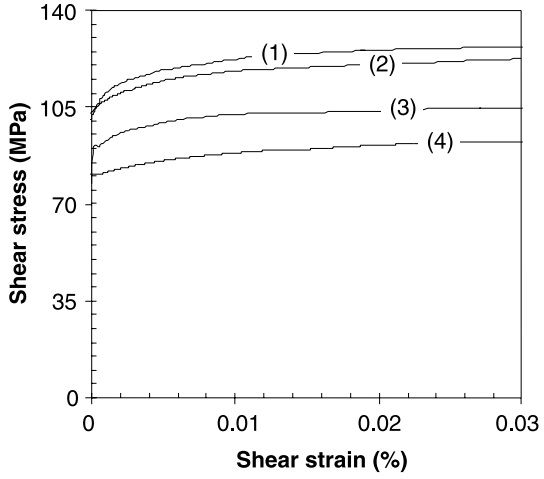

Fig. 8. Simulations of forest hardening: influence of the prismatic forest on the stress–strain curve for edge and screw dislocations at $T = 300$ K and with an imposed strain rate of 10^{-5} s^{-1}. (1) Screw dislocation line interacting with a prismatic forest. (2) Screw dislocation line in the absence of forest. (3) Edge dislocation line interacting with a prismatic forest. (4) Edge dislocation line in the absence of forest.

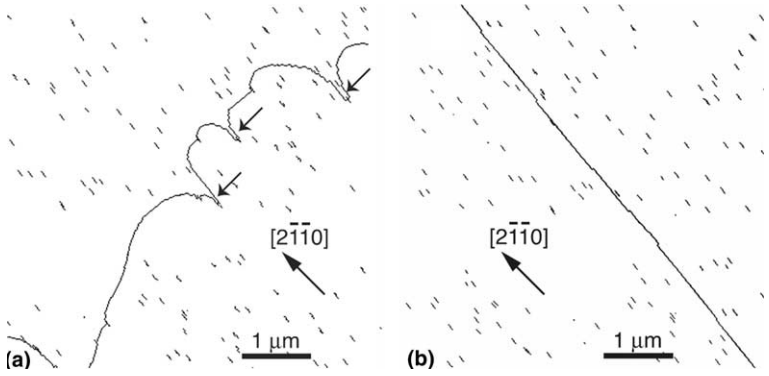

Fig. 7. Simulations of forest hardening. Thin foils of thickness 0.2 μm extracted from the simulation cell. The forest dislocations of screw character intersect the slip plane with an average spacing of 1 μm. The initial character of the mobile line is edge (a) or screw (b). Notice in (a) the short screw segments formed near the junctions (arrows).

or absence of a forest density. The stress levels reached with edge dislocations depend on their mobility. Thus, they depend on the constitutive assumptions made in Section 3.2. What matters, however, is the difference recorded in the presence or absence of a forest density.

With an initially edge dislocation line, a significant hardening is obtained. A moderate forest density of $\rho_f = 10^{12}$ m^{-2} induces in the present case a stress increase of 12 MPa at 300 K. In comparison, the hardening recorded for screw lines does not exceed 3 MPa. This simple example confirms that the motion of screw dislocations is weakly sensitive to the presence of a prismatic forest. In the absence of junctions, the increase in flow stress recorded for screw dislocations does not result from line tension effects. It arises from a local decrease in dislocation mobility due to superkink formation upon elastic interactions with obstacles at small approach distances (Fig. 7(b)). Under a constant imposed dislocation mobility, the corresponding reduction in the free-length of the screw segments results in a rather small hardening according to Eq. (5). Indeed, a small stress increase in the exponential term is sufficient to compensate for the decrease of the prefactor.

5. Discussion

As was shown in Figs. 4 and 5, the sensitivity of the flow stress to temperature and strain rate can be properly reproduced provided that the stress vs. velocity law for screw dislocations is known and that the screw mobility is low compared to that of edges. Thus, prismatic slip of dislocations in pure Zr at low temperature is entirely determined by the strong lattice friction on screw dislocations. Since the physical origin of solute hardening is still a matter of debate (see [6,9]), it is accounted for by lumping it into the velocity rule for screw dislocations. There is also an interaction between non-screw segments and impurities, which can be accounted for by the mobility law for non-screw dislocations. However, this interaction is not strong enough to prevent the formation of long screw segments at low temperature.

The strain hardening produced by the interaction of prismatic slip systems at low temperature is unexpectedly small. The two approaches used here, namely the mapping of equilibrium configurations of interacting dislocations and the simulations of forest hardening, provide results that are consistent with the simulated microstructures. While edge dislocations form junctions with forest dislocations of all characters, the interaction between screw dislocations never results in junction formation. As a consequence, the low temperature hardening is rather moderate, since it only involves non-contact interactions. One may note that it was not estimated here using a Taylor-type relationship between flow stress and the square root of forest density. Indeed, as was shown experimentally by Keh and Weissmann in the case of alpha-iron [38] and further checked in a simulation study of bcc crystals at low temperature [32], the Taylor relation does not apply to forest hardening in the presence of strong Peierls forces. This relation is in fact only valid for dislocations that bow out under stress and take equilibrium shapes between forest obstacles. In contrast, screw dislocation still move as straight lines in the same conditions (compare Fig. 7(a) and (b)).

The simulated stress–strain curves actually exhibit a hardening that is smaller than the one predicted by model simulations of forest hardening, or even a small softening (Fig. 5). This is due to the multiplication of screw dislocations in the absence of obstacles that can significantly reduce their mobility with increasing strain. Thus, single crystals of Ti or Zr deformed in conditions of single or duplex slip on prismatic planes are expected to show a rather flat initial deformation stage as long as other slip systems are not activated. Experimental evidences obtained in such conditions are available for both Ti [9] and Zr crystals (Fig. 9). This figure shows the stress–strain curve of a Zr single crystal containing 400 wt. ppm of oxygen at 300 K. The orientation of the stress axis is close to the one investigated here, but such that a single prismatic slip plane is activated with a Schmid factor of 0.46 (J. Crepin, unpublished work). A kind of easy glide behavior is obtained, with practically no measurable strain hardening. At larger strains, a stage with stronger hardening is observed, which is associated with the onset of first-order pyramidal slip and the observation of cross-slipped traces at the surface of the deformed crystals. In spite of the analogy that is often made between the low temperature properties of bcc metals and hcp metals deforming by prismatic slip, the stress–strain responses appear, thus, to be quite

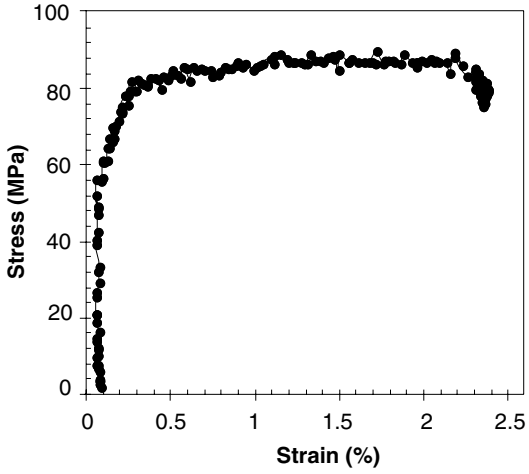

Fig. 9. Stress–strain curve of a Zr crystal in easy glide conditions at $T = 300$ K and with an imposed strain rate of 2×10^{-4} s^{-1}. After J. Crépin (unpublished work), by courtesy.

different. No well-defined stages are found in bcc crystals, due to stronger forest interactions and the continuous production of forest density by the easy motion of non-screw segments in many slip planes. Therefore, the low temperature stress–strain curves associated with prismatic slip in hcp metals are unique and combine features typical of both bcc and fcc crystals.

The present results suggest two directions for future developments. As far as prismatic hardening is concerned, the absence of forest hardening may lead to the consideration of less efficient hardening mechanisms that are usually neglected. The formation of jogs upon dislocation intersections is not accounted for in the present simulations and could be implemented. Perhaps more relevant to the present study is another jog hardening mechanism that is typically associated with lattice friction. The jogs are mobile in the $\{0001\}$ basal plane and are dragged by the screw dislocations. They can also block kinks moving along the dislocation lines, which contributes to a further reduction of the free-length of the screw segments by a mechanism similar to the one described in Section 4.4.2. A strong pinning effect is, nevertheless, not expected since this would contradict the experimental observation of long straight screw segments.

Finally, the activation of first-order $\langle a \rangle$ pyramidal slip results in the occurrence of a hardening stage akin to stage II behavior in fcc single crystals. DD simulations, using the methods developed in the present study, can perform an investigation of the resulting forest interactions. The main difficulty resides in the extreme scarcity of the experimental or theoretical results on dislocation glide in secondary slip systems.

6. Conclusion

This paper presents the first simulation of DD in single crystals of hcp transition metals, like Zr or Ti, which preferentially deform by prismatic slip. The crystallographic structure was reproduced using an orthorhombic representation of the hexagonal lattice. This allowed transposing without major modifications existing DD simulations developed for cubic materials. The emphasis being on low temperature properties, a methodology was developed to control the mean-free path of the highly mobile non-screw dislocations. As the available models provide guidelines but no numerical predictions, the mobilities of screw and non-screw segments were defined in a phenomenological manner. Several investigations were performed on the hardening that results from the interactions of dislocations gliding in different prismatic slip planes. The net result is that no junctions can be formed between intersecting screw dislocations, so that the work hardening coefficient drops to rather small values when temperature decreases and the microstructure increasingly consists of long screw segments. This explains experimental observations of an initial deformation stage with a low strain hardening coefficient during the low temperature deformation of Ti or Zr. Thus, the thermally activated mobility of screw dislocations in zirconium does not influence only the arrangement of the dislocation microstructures but also the strain hardening properties. Finally, this work shows that in spite of the lack of predictive models for dislocation mobilities, it is still possible to carry out controlled simulations of hardening properties and obtain from them some meaningful physical insight.

Acknowledgements

The authors are grateful to Dr. J. Crépin for providing his experimental results prior to publication.

References

[1] Rapperport EJ, Hartley CS. Trans Metall Soc AIME 1960;218:869.
[2] Reed-Hill RE. In: Reed-Hill RE, Hirth JP, Rogers HC, editors. Deformation Twinning, vol. 25. Warrendale (PA, USA): TMS; 1964. p. 295.
[3] Akhtar A. Met Trans A 1975;6:1217.
[4] Tomé CN, Lebensohn RA, Kocks UF. Acta Metall Mater 1991;39:2667.
[5] Fundenberger JJ, Philippe MJ, Wagner F, Esling C. Acta Mater 1997;45:4041.
[6] Ferrer F. PhD thesis, Ecole Polytechnique, Palaiseau, France 2000.
[7] Soo P, Higgins GT. Acta Met 1968;16:177.
[8] Mills D, Craig GB. Trans Metal Soc AIME 1968;242:1881.
[9] Naka S, Lasalmonie A, Costa P, Kubin LP. Phil Mag A 1988;57:717.
[10] Caillard D, Couret A. Mater Sci Eng A 2002;322:108.
[11] Legrand B. Phil Mag A 1984;52:83.
[12] Bacon DJ, Vitek V. Metall Mater Trans A 2002;33:721.
[13] Seeger A, Schiller P. Acta Met 1962;10:348.
[14] Schoeck G. Phys Stat Sol 1965;8:499.
[15] Levine ED. Trans JIM 1968;9:832.
[16] Devincre B. In: Kirchner HO, Pontikis V, Kubin LP, editors. Computer Simulation in Materials Science. Amsterdam, North-Holland: Kluwer Academic Publishers; 1996. p. 309.
[17] Devincre B, Kubin LP, Lemarchand C, Madec R. Mater Sci Eng A 2001;309–310:211–9.
[18] Schwarz KW. J Appl Phys 1999;85:108–19.
[19] Zbib HM, Rhee M, Hirth JP. Int J Mech Sci 1998;40:113–27.
[20] Ghoniem NM, Tong SH, Sun LZ. Phys Rev B 2000;139(2):913–27.
[21] Madec R, Devincre B, Kubin LP. In: Kubin LP, Selinger RL, Bassani JL, Cho K, editors. Multiscale modeling of materials – 2000, Symp Proc vol 653. Warrendale (PA, USA): Materials Research Society; 2001. p. Z1.8.1.
[22] Devincre B, Condat M. Acta Metall Mater 1992;40:2629.
[23] Foreman AJE. Phil Mag 1967;15:1011–21.
[24] Madec R, Devincre B, Kubin LP. Phys Rev Lett 2002;89(25):255508.
[25] Otte HM, Crooker AG. Phys Stat Sol 1965;9:441.

[26] Henry NFM, Lonsdale K. International tables for X-ray crystallography. Birmingham: The Kynoch Press; 1969. p. 19.
[27] Bulatov VV, Rhee M, Cai W. In: Kubin LP, Selinger RL, Bassani JL, Cho K, editors. Multiscale modeling of materials – 2000, Symp Proc vol 653. Warrendale (PA, USA): Materials Research Society; 2001. p. Z1.3.1.
[28] Madec R, Devincre B, Kubin LP. In: Proceedings of IUTAM Symposium on Mesoscopic Dynamics in Fracture Process and Strength of Materials. Amsterdam, North-Holland: Kluwer Academic Publishers, in press.
[29] Devincre B, Roberts S. Acta Metall 1996;74:2891.
[30] Tang M, Kubin LP, Canova GR. Acta Mater 1998;46:3221.
[31] Kocks UF, Argon AS, Ashby MF. Thermodynamics and kinetics of slip. Prog Mater Sci 1975;19:1.
[32] Tang M, Devincre B, Kubin LP. Modelling Simul Mater Sci Eng 1999;7:893–908.
[33] Tyson WR. Canad Met Quart 1968;6:301.
[34] Kubin LP, Madec R, Devincre B. In: Zbib HM, Lassila DH, Levine LE, Hemker KJ, editors. Multiscale Phenomena in Materials, Symp Proc vol 779. Warrendale (PA, USA): Materials Research Society; 2001. p. 25.
[35] Wickham LK, Schwarz KW, Stölken JS. Phys Rev Lett 1999;83:4574–7.
[36] Madec R, Devincre B, Kubin LP. Computat Mater Sci 2002;23:219–24.
[37] Kroupa F. Czech J Phys B 1961;11:847.
[38] Keh AS, Weissmann S. In: Thomas G, Washburn J, editors. Microscopy and strength of crystals. New York: Interscience; 1963. p. 231.